ChemComm

COMMUNICATION

View Article Online
View Journal

Cite this: DOI: 10.1039/d6cc01252c

Received 28th February 2026,
Accepted 27th April 2026

DOI: 10.1039/d6cc01252c

rsc.li/chemcomm

Factors maximising photoinduced electron-transfer-coupled phase migration to boost biphasic photocatalysis

Ren Itagaki,[a] Akinobu Nakada, *[ab] Hajime Suzuki,[ac] Osamu Tomita[a] and Ryu Abe *[a]

The use of biphasic solutions has recently attracted attention as an effective strategy to spatially extend photoinduced charge separation between the photocatalyst and electron donors/acceptors *via* phase migration, enabling efficient photocatalysis. Herein, key parameters of biphasic photocatalytic systems, namely, diffusion in solution, liquid–liquid phase boundary, and phase transfer equilibrium, were modulated in detail, unveiling design principles that maximise the benefits of biphasic systems.

Photoinduced electron transfer and charge separation are among the most common and essential driving principles of redox-based photocatalytic molecular conversions, such as CO_2 reduction,[1] water splitting[2] and organic transformations.[3] Since the product of photon absorption efficiency, charge-separation fraction, and survival yield against charge recombination determines the overall reaction quantum efficiency, many studies have focused on photoinduced charge separation and recombination.[4–6]

Recently, photocatalysis in immiscible biphasic solutions has been demonstrated to spatially facilitate charge separation and suppress backward electron transfer (recombination).[7] In a biphasic solution, a key mechanism enabling spatial charge separation is interphase migration triggered by photoinduced electron transfer (Fig. 1),[8] which is inspired by electrochemically well-studied electron-transfer-coupled phase-transfer phenomena observed for reversible redox couples such as ferrocenium (Fc^+)/ferrocene (Fc),[9] benzoquinone/hydroquinone,[10] 7,7,8,8-tetracyanoquinodmethane (TCNQ),[11] and alkyl viologens.[12] In Fig. 1, electron

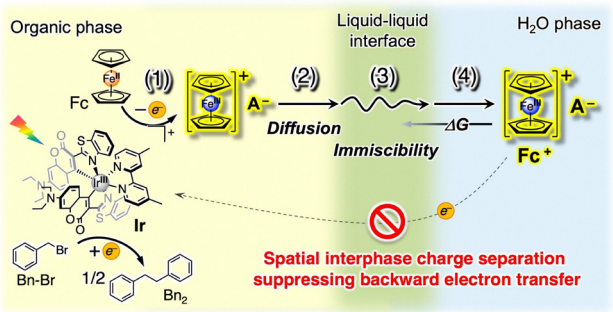

Fig. 1 Schematic illustration of biphasic photocatalysis driven by photoinduced electron-transfer-coupled phase migration.

transfer between a photoexcited Ir(III) complex photoredox catalyst (**Ir**) and Fc as an electron donor produces a charge-separated pair of reduced **Ir** and Fc^+ in the organic solution phase (process (1) in Fig. 1). Because the generated Fc^+ in the organic phase has a completely different solubility from that of water-insoluble Fc, migration of Fc^+ to the counterpart aqueous solution phase proceeds (processes (2) and (3)), enabling interphase charge separation. This photoinduced electron-transfer-coupled phase migration has been demonstrated to suppress backward electron transfer effectively.[7] Furthermore, challenging artificial photosynthetic reactions that connect water oxidation and reductive molecular conversion (*i.e.*, H_2 evolution[13] and organic transformation[14]) have been demonstrated using a biphasic solution and photoinduced phase migration.

In addition to the conventional photoredox steps that generate a charge-separated pair (process (1) in Fig. 1) and its diffusion (process (2)), interfacial mass transport across the liquid–liquid boundary (process (3)) and phase transfer equilibrium (process (4)) are involved in biphasic photocatalysis; these additional parameters should affect the overall photocatalytic efficiency. However, the biphasic properties that most strongly control the photoreaction outcome remain unclear. Herein, we modulated diffusion in solution, immiscibility

[a] *Department of Energy and Hydrocarbon Chemistry, Graduate School of Engineering, Kyoto University, Nishikyo-ku, Kyoto 615-8510, Japan. E-mail: nakada@tmu.ac.jp, ryu-abe@scl.kyoto-u.ac.jp*

[b] *Department of Applied Chemistry for Environment, Graduate School of Urban Environmental Sciences, Tokyo Metropolitan University, 1-1 Minami-Osawa, Hachioji, Tokyo 192-0397, Japan*

[c] *Precursory Research for Embryonic Science and Technology (PRESTO), Japan Science and Technology Agency (JST), 4-1-8 Honcho, Kawaguchi, Saitama 332-0012, Japan*

Table 1 Photophysical properties of **Ir** in each solvent

Solvent	ε^a	μ^b /mPa s	λ_{abs}/nm	$\lambda_{em}{}^c$/nm	$\tau_0{}^d$/μs	k_q/ 10^9 M^{-1} s^{-1}	$\eta_q{}^e$/%
DCM	8.9	0.41	483	588	26.1	9.6	>99
DCE	10.4	0.78	482	590	25.6	6.7	>99
DCB	9.9	1.32	487	590	19.2	8.6	>99
MeCN	36.7	0.34	478	588	3.6	8.6	>99

[a] Dielectric constant at 25 °C.[17] [b] Viscosity at 25 °C.[18] [c] Excitation at 480 nm. [d] Excitation at 440 nm. [e] Quenching efficiency when [Fc] = 5 mM.

between the two liquid phases, and partition equilibrium to elucidate the factors that maximise photoinduced phase migration and boost biphasic photocatalysis.

The UV-visible absorption and emission properties of **Ir** in organic solvents are summarised in Table 1. In each solvent, **Ir** exhibited an intense visible absorption band assigned to ligand-centred charge-transfer transitions,[15,16] with only minor solvent dependence (Fig. S1a). Under deaerated conditions, **Ir** displayed room-temperature phosphorescence with a maximum at ~590 nm (Fig. S1a), and its lifetime decreased markedly in acetonitrile (MeCN) compared with that in halogenated solvents because of differences in their dielectric constants (Table 1 and Fig. S1b), as previously reported.[15,16]

The incremental addition of Fc led to a decrease in the emission intensity of **Ir**, suggesting reductive quenching (Fig. S1c–f). Stern–Volmer analysis (see SI) provided quenching rate constants k_q on the order of 10^9 M^{-1} s^{-1}, consistent with near diffusion-controlled quenching. The efficiency of reductive quenching (η_q) of photoexcited **Ir** by Fc was almost quantitative at [Fc] = 5 mM (Table 1). Therefore, [Fc] was fixed at 5 mM for the photocatalytic evaluation to eliminate differences in the photoinduced electron process.

In each organic solvent, Fc showed a reversible wave attributed to a metal-centred Fe(III/II) redox process at $E_{1/2}$ ~ 0.09–0.25 V *vs.* Ag/$AgNO_3$ (Fig. S2a–d). The diffusion coefficient (D) of Fc, which was estimated from the Randles–Sevcik plots (see SI), decreased in the order MeCN > dichloromethane (DCM) > 1,2-dichloroethane (DCE) > 1,2-dichlorobenzene (DCB), following the Stokes–Einstein relationship with viscosity (μ^{-1}) (Fig. S2f). Difference in diffusion in the organic solution may affect the opportunity to reach the liquid–liquid interface (process (2) in Fig. 1) before interphase charge separation in biphasic photocatalysis, as discussed later.

The immiscibility of the two solvent phases is an important biphasic characteristic that likely affects the migration across the liquid–liquid boundary (process (3) in Fig. 1). In this study, we used the solubility of an organic solvent (1 mL) in the same volume of water (1 mL) as a pseudo-parameter to describe immiscibility (Table S1 and Fig. S3). Pure MeCN is almost completely miscible with water at a concentration of approximately 4 M (Table S1). Upon addition of $(NH_4)_2SO_4$ to the MeCN/water mixed solvent, a biphasic solution was formed owing to the salting-out effect.[19] The solubility of MeCN decreased with increasing $(NH_4)_2SO_4$ concentration (Table S1). The solubility of the halogenated solvents in water was several orders of magnitude lower than that of MeCN, even when 2 M $(NH_4)_2SO_4$ was added.

The partition coefficients in the H_2O/DCE biphasic solution (C_{H_2O}/C_{DCE}; C_X indicates the concentration in phase X) of each compound were estimated to be 2×10^{-5} (Fc), 1×10^{-6} (**Ir**), 1×10^{-6} (Bn–Br), and 122 (Fc^+Cl^-), based on the absorption spectra of each phase of the biphasic solution after reaching equilibrium (Fig. S4a and Table S2). Thus, the starting compounds for photoredox catalysis were initially predominantly distributed in the DCE phase, whereas Fc^+Cl^- showed a strong preference for the aqueous phase. The partitioning trends were similar for MeCN/H_2O salted-out with 2 M $(NH_4)_2SO_4$ (Fig. S4b and Table S2).

Visible-light irradiation of a biphasic H_2O/DCE solution (2.0 mL) containing Fc (5.0 mM), **Ir** (0.05 mM), and benzyl bromide (Bn–Br, 50 mM), all of which were predominantly distributed in the DCE phase, with stirring under Ar (λ = 470 nm) produced Fc^+ and dibenzyl (Bn_2) in the aqueous and DCE phases, respectively, at a stoichiometric ratio satisfying eqn (1) (Fig. 2 and S5, and Entry 1 in Table S3).

$$Fc + Bn\text{–}Br \rightarrow Fc^+ + 1/2Bn_2 + Br^- \quad (1)$$

where the entire reaction involves the photocatalytic reduction of Bn–Br using Fc as an electron donor. In contrast, no product was obtained in the absence of the aqueous phase (Entry 2 in Table S3). We previously reported that Fc^+ remaining in the DCE phase inhibits further production of Fc^+ *via* backward electron transfer (*i.e.* re-reduction of Fc^+ to Fc), whereas Fc^+ that migrates to the aqueous phase does not, owing to spatial charge separation across the liquid–liquid interface (see Fig. 1).[7] Hence, escape of the generated Fc^+ from DCE to the aqueous phase was the key to suppressing backward electron transfer and promoting the photocatalytic reaction. Accordingly, the amount of Fc^+ generated in the reaction system was used as an indicator of photocatalytic performance.

The effect of forming a biphasic solution was systematically examined in a MeCN/H_2O system with different concentrations

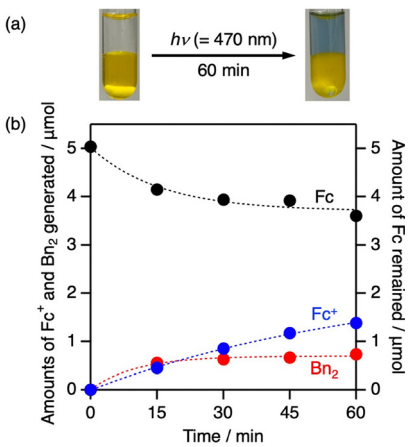

Fig. 2 (a) Photographs of a biphasic solution before and after irradiation, and (b) time course of Fc^+/Bn_2 formation and Fc consumption along with Fc conversion from a biphasic H_2O/DCE solution (1 : 1, *v*/*v*; 2.0 mL) containing Fc (5.0 mM, 5 μmol), **Ir** (0.05 mM, 50 nmol), and Bn–Br (50 mM, 50 μmol) under visible-light irradiation (λ = 470 nm).

of $(NH_4)_2SO_4$ (Fig. 3a and Table S3). Similar to single-phase DCE system, a single-phase MeCN–H_2O mixed solution without $(NH_4)_2SO_4$ did not generate any products (Entry 3 in Table S3). In contrast, upon addition of $(NH_4)_2SO_4$ to the MeCN–H_2O mixture to induce phase separation, Fc^+ was generated under visible-light irradiation (entries 4–7 in Table S3). The amount of Fc^+ increased with increasing $(NH_4)_2SO_4$ concentration, owing to the increased immiscibility of the MeCN/H_2O system (Fig. 3a). Even in macroscopically phase-separated systems, partial mixing can occur in the interfacial region. The extent of this mixing depends on the mutual solubility of the two phases. If the mixed boundary has properties similar to those of a miscible solvent, recombination of the charge-separated pair can be accelerated before escape to another phase (process (3) in Fig. 1). Hence, it was concluded that decreasing the mutual solubility of the two phases by salting-out with $(NH_4)_2SO_4$ improved the photocatalytic activity.

Halogenated solvent/H_2O biphasic systems, in which the immiscibility was much higher than in the MeCN/H_2O system, exhibited much higher photocatalytic activities (Fig. 3a). Note that the noticeable difference in their behaviour was not found during mixing among biphasic solutions used in this study (Supplementary movies). Upon closer inspection, however, the activity (DCM > DCE > DCB) did not correlate with immiscibility in water (DCB > DCE > DCM). The diffusion coefficient (D) of Fc^+ in the halogenated solvent explained the photocatalytic trend (Fig. 3b); rapid diffusion in the organic phase possibly increased the opportunity for Fc^+ to reach the interphase boundary for phase migration, enabling spatial charge separation (process (2) in Fig. 1). Because the immiscibility of the halogenated solvent/H_2O was sufficiently high, the effects of D likely became another significant factor. In contrast, although D in MeCN was larger than that in any halogenated solvent employed in this study, the photocatalytic activity was much lower, likely because the significantly low immiscibility of MeCN with H_2O was the dominant limiting factor. It should be noted that the immiscibility of the halogenated solvents was further improved by addition of $(NH_4)_2SO_4$, which resulted in a slight but obvious increase in photocatalytic activity (Fig. 3b). Thus, it was concluded that both immiscibility and diffusion are important factors.

For salting-out, the salt (*i.e.*, $(NH_4)_2SO_4$ in this work) dissolved in water plays a crucial role in decreasing the solubility of the counterpart organic solvent.[19] Here, the additional effects of a salt "dissolved in the organic phase" were also investigated on biphasic photocatalytic efficiency. As has been used in phase transfer catalysis, tetrabutylammonium cation enables hydrophilic anions to be distributed in the organic solution phase.[20] In fact, the majority of tetrabutylammonium hydrogen sulfate ($TBAHSO_4$) partitioned in the DCE and MeCN phases in H_2O/DCE (C_{H_2O}/C_{DCE} = 0.11) and salted-out MeCN/H_2O (C_{H_2O}/C_{MeCN} ~ 0) biphasic solutions (Table S2 and Fig. S6). In the H_2O/DCE biphasic system, $TBAHSO_4$ markedly enhanced photocatalytic activity (Fig. 4a). Notably, $TBAHSO_4$ did not make MeCN/H_2O solution biphasic, indicating it has no role of salting-out. Combined addition of $TBAHSO_4$ and $(NH_4)_2SO_4$ further improved photocatalytic efficiency. In contrast, the promotional effect of $TBAHSO_4$ was observed only in the presence of $(NH_4)_2SO_4$ in the MeCN/H_2O system; addition of $TBAHSO_4$ alone resulted in no activity (Fig. 4b). These results suggest different roles for $TBAHSO_4$ and $(NH_4)_2SO_4$ in promoting photocatalysis, and that $TBAHSO_4$ is likely to promote interphase charge separation.

Phase migration of Fc^+ generated by photoinduced electron transfer in the organic phase occurs with an anion A^- to maintain charge balance in the solution phase. Hence, the driving force for phase transfer, represented by $\Delta G(Fc^+A^-)_{Org\rightarrow H_2O}$ (eqn (2)) is a key factor that can be tuned using coexisting anions in the organic phase.

$$\Delta G(Fc^+A^-)_{Org\rightarrow H_2O} = \Delta G(Fc^+)_{Org\rightarrow H_2O} + \Delta G(A^-)_{Org\rightarrow H_2O} \quad (2)$$

For the H_2O/DCE system, the Gibbs energy for ion migration of Fc^+ from the DCE phase to the aqueous phase ($\Delta G(Fc^+)_{DCE\rightarrow}$

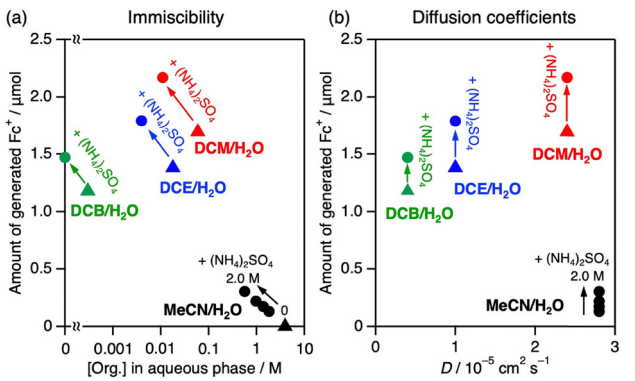

Fig. 3 Amounts of photochemically generated Fc^+ in biphasic solutions containing Fc (5.0 mM, 5 μmol), **Ir** (0.05 mM, 50 nmol), and Bn–Br (50 mM, 50 μmol) under visible-light irradiation (λ = 470 nm, 60 min) against (a) the concentration of each organic phase solvent dissolved in the aqueous phase ([Org.] in aqueous phase) and (b) the diffusion coefficient (D) of Fc in each organic phase in the presence and absence of various concentrations of $(NH_4)_2SO_4$.

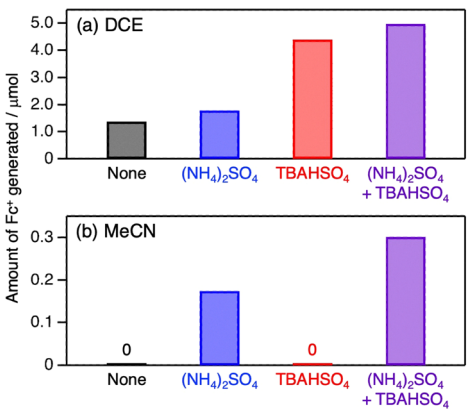

Fig. 4 Amount of Fc^+ generated in biphasic (a) H_2O/DCE and (b) MeCN/H_2O solutions containing Fc (5.0 mM, 5 μmol), **Ir** (0.05 mM, 50 nmol), and Bn–Br (50 mM, 50 μmol) under visible-light irradiation (λ = 470 nm, 60 min) in the presence and absence of $(NH_4)_2SO_4$ (2.0 M) and/or $TBAHSO_4$ (5.0 mM).

$_{H_2O}$) was reported to be −2.0 kJ mol^{-1}.[21] The presence of HSO_4^- in the DCE phase ($\Delta G(HSO_4^-)_{DCE\rightarrow H_2O}$ = −46 kJ mol^{-1})[22] substantially increased the driving force for phase migration. Once Fc^+A^- migrates to the aqueous phase, it still has the opportunity to kinetically return to the DCE phase during the photocatalytic reaction owing to the distribution equilibrium (process (4) in Fig. 1). Therefore, we conclude that addition of $TBAHSO_4$, by improving $\Delta G(A^-)_{Org\rightarrow H_2O}$, further decreases backward charge recombination in the organic phase, thereby increasing photocatalytic efficiency.

In summary, we elucidated the key factors that maximise recently emerged biphasic photocatalysis *via* phase migration by modulating chemical parameters, including diffusion in solution, immiscibility, and the driving force for phase transfer, using Fc^+/Fc phase-migrating electron mediators. The first key factor is the immiscibility of the two solution phases. Formation of a biphasic solution is essential to enable spatial charge separation between the two liquid phases, thereby suppressing backward electron transfer. Upon decreasing the mutual solubility of the solutions to construct biphases, interphase charge separation accelerated (process (3) in Fig. 1). On the premise of high immiscibility in the biphasic solution, high diffusion coefficients of the electron mediator in the bulk solution improved biphasic photocatalysis owing to an increased opportunity to reach the phase boundary and escape to the other solution phase (process (2) in Fig. 1). Finally, a large driving force for phase migration of the electron mediator, which can be controlled by escorting counter-ions, plays an important role in suppressing backward phase migration. This work provides design principles for constructing photoinduced electron-transfer-driven interphase charge transport in biphasic photocatalysis, which is promising for achieving artificial photosynthetic reactions coupled with valuable oxidative and reductive molecular conversions.[13,14]

Conflicts of interest

There are no conflicts to declare.

Data availability

The data supporting this article have been included as part of the supplementary information (SI). Supplementary information: cyclic voltammograms, UV-vis absorption and emission spectra, HPLC chromatograms, concentration of organic solvents in D_2O, ^{1}H NMR spectra (PDF). See DOI: https://doi.org/10.1039/d6cc01252c.

Acknowledgements

This work was supported by JSPS KAKENHI grants (JP24K01603, JP26K21755, and JP26K01622) and a Grant-in-Aid for Transformative Research Areas ''Concerto Photocatalysis'' (JP23H03830 and JP23H03832) R.I. wishes to acknowledge the support from JSPS Fellowship for Young Scientists (JP23KJ1351).

References

1 Y. Yamazaki, H. Takeda and O. Ishitani, *J. Photochem. Photobiol., C*, 2015, **25**, 106–137.
2 Y. Wang, H. Suzuki, J. Xie, O. Tomita, D. J. Martin, M. Higashi, D. Kong, R. Abe and J. Tang, *Chem. Rev.*, 2018, **118**, 5201–5241.
3 C. K. Prier, D. A. Rankic and D. W. C. MacMillan, *Chem. Rev.*, 2013, **113**, 5322–5363.
4 D. M. Arias-Rotondo and J. K. McCusker, *Chem. Soc. Rev.*, 2016, **45**, 5803–5820.
5 C. Wang, H. Li, T. H. Burgin and O. S. Wenger, *Nat. Chem.*, 2024, **16**, 1151–1159.
6 N. Hosokawa, K. Ozawa, K. Koike, Y. Tamaki and O. Ishitani, *Chem. Sci.*, 2025, **16**, 4279–4289.
7 R. Itagaki, S. Takizawa, H.-C. Chang and A. Nakada, *Dalton Trans.*, 2022, **51**, 9467–9476.
8 Z. Samec, *Pure Appl. Chem.*, 2004, **76**, 2147–2180.
9 A. D. Pendergast, S. Gutierrez-Portocarrero, R. Noriega and H. S. White, *J. Am. Chem. Soc.*, 2024, **146**, 30464–30473.
10 H. Moon and J. H. Park, *Anal. Chem.*, 2021, **93**, 16915–16921.
11 Z. Ding and P. F. Brevet, *Chem. Commun.*, 1997, 2059–2060.
12 J. Hanzlík and Z. Samec, *Collect. Czech. Chem. Commun.*, 1987, **52**, 830–837.
13 Y. H. Hong, Y. M. Lee, W. Nam and S. Fukuzumi, *J. Am. Chem. Soc.*, 2022, **144**, 695–700.
14 R. Itagaki, A. Nakada, H. Suzuki, O. Tomita, H.-C. Chang and R. Abe, *J. Am. Chem. Soc.*, 2025, **147**, 15567–15577.
15 S. Takizawa, N. Ikuta, F. Zeng, S. Komaru, S. Sebata and S. Murata, *Inorg. Chem.*, 2016, **55**, 8723–8735.
16 S. Sebata, S. Takizawa, N. Ikuta and S. Murata, *Dalton Trans.*, 2019, **48**, 14914–14925.
17 A. A. Maryott and E. R. Smith, *Table of Dielectric Constants of Pure Liquids*, National Bureau of Standards, Washington, D.C., 1951.
18 Y. Marcus, *The Properties of Solvents*, Wiley, Chichester, 1998.
19 A. M. Hyde, S. L. Zultanski, J. H. Waldman, Y.-L. Zhong, M. Shevlin and F. Peng, *Org. Process Res. Dev.*, 2017, **21**, 1355–1370.
20 C. M. Starks, *J. Am. Chem. Soc.*, 1971, **93**, 195–199.
21 J. Hanzlik, Z. Samec and J. Hovorka, *J. Electroanal. Chem.*, 1987, **216**, 303–308.
22 T. G. Henares, J. D. Gale, G. Herzog and D. W. M. Arrigan, *ChemElectroChem*, 2022, **9**, e202200681.